A Model of Polymeric Nanopropulsion Engine

Jan-Michael Y. Carrillo,[†] JunHwan Jeon,[‡] and Andrey V. Dobrynin*,[†]

Polymer Program, Institute of Materials Science and Department of Physics, University of Connecticut, Storrs, Connecticut 06269, and Department of Chemical Engineering, Vanderbilt University, Nashville, Tennessee 37235

Received March 13, 2007; Revised Manuscript Received April 24, 2007

ABSTRACT: We have performed molecular dynamics simulations and developed a scaling model of a nanopropulsion engine. The engine consists of a nozzlelike pore with catalytic sites located at the closed end of the nozzle. The nozzle is immersed in a solution of monomers that serves as a "fuel" for the polymerization reaction. The engine can be thought of as an analogue of the jet propulsion engine that secretes polymers in a solution and utilizes polymer viscoelasticity for its motion. Using scaling analysis, we have established that the nozzle velocity is proportional to the chain's polymerization rate with the proportionality coefficient being determined by the nozzle geometry, the nozzle friction coefficient, and the dynamics of the polymer chains inside the nozzle. The results of the molecular dynamics simulations are in remarkable agreement with the predictions of the scaling model.

Molecular motors are machines that convert chemical energy to mechanical energy and force.[1−9] Molecular motors in nature are used to transport biochemicals and provide motility to the cells. For example, the kinesin protein moves along microtubules carrying chemical payloads by converting the energy released upon ATP hydrolysis into mechanical work.[8] A flagellar biological motor provides motility to bacteria through a whiplike rotary motion.[10,11] Many intracellular pathogens such as *Listeria* propel themselves by assembling the host cell actin into a cometlike tail of cross-linked filaments.[5,12,13] Another fascinating example of molecular machinery is the gliding of cyanobacteria and myxobacteria on surfaces, which is accompanied by a steady secretion of gel (slime) from nozzlelike pores.[5,7,14] These complex machines serve as an inspiration for design of artificial devices capable of transporting "cargo" in chip size laboratories for future nanotechnological applications.[11,15−22]

In this paper we study a simple model of a polymeric nanopropulsion engine, which generates a self-propelling motion via polymerization within a nozzlelike pore. We consider a cylindrical pore with one end of the pore being closed by a circular cap, as shown in Figure 1. A circular cap contains catalytic sites that facilitate polymerization of macromolecules inside a nanonozzle. The nozzle is immersed in a solution of monomers that serves as a "fuel" for the polymerization reaction. The physical principle for the operation of this engine is very simple and is based on the viscoelastic nature of polymeric liquids.[23−26] Addition of new monomers to a polymer chain induces a local stress in the polymeric liquid confined inside the nozzle. The response of a polymeric liquid to an external perturbation strongly depends on a rate with which this perturbation is applied. In our case this external perturbation is the addition of a new monomer (taken from outside the nozzle) to a polymer chain, growing inside the nozzle. If addition of a monomer to a polymer chain occurs faster than the relaxation time of chain sections confined inside the nozzle, it results in the chain's compression, which generates an osmotic force acting on the nozzle cap pushing the nozzle forward. However, only a fraction of the free energy stored during the chain's polymerization is used for the propulsive motion while the rest is dissipated as friction when the polymeric liquid moves through the nozzle and the nozzle moves through the solvent. The energy partitioning depends on the chain polymerization rate, solution viscosity, and nozzle geometry. Indeed, our simulations and scaling analysis of the nozzle motion show that the nozzle velocity is proportional to the net polymerization rate with a proportionality coefficient being determined by the geometric characteristics of the nanonozzle.

To test the design idea of the nanopropulsion engine, we performed coarse-grained molecular dynamics simulations of a nozzle with growing inside polymer chains immersed in a solution of monomers. These simulations correspond to the Zimm dynamics of the nanonozzle.[23−26] In our simulations, a nanonozzle was modeled by an end-capped tube (see Figure 2). The cylindrical surface of the tube was formed by wrapping hexagonally packed sheet consisting of $C \times L$ monomers, where C is the number of monomers forming the circumference of the tube and L is the number of monomers along the tube axis. One end of the tube was closed by flat circular cap with C monomers in its circumference. Each monomer on the tube surface was connected to its six neighbors by elastic bonds which elasticity is described by the finite extension nonlinear elastic (FENE) potential

$$U_{\mathrm{FENE}}(r) = -0.5K_s{R_{\max}}^2 \ln\left(1 - \frac{r^2}{{R_{\max}}^2}\right) \qquad (1)$$

where K_s is the spring constant, $K_{s,\mathrm{tube}} = 30k_BT/\sigma^2$ (k_B is the Boltzmann constant, T is the absolute temperature, and σ is the bead diameter), r is the distance between the center of mass of two neighboring beads, and the maximum bond length is $R_{\max} = 1.5\sigma$. The growing polymer chains were modeled by bead−spring chains with the spring constant, $K_{s,\mathrm{polymer}} = 30k_BT/\sigma^2$. In addition to the FENE potential, all beads in the system including solvent molecules interact through the truncated-

* Corresponding author. E-mail: avd@ims.uconn.edu.
[†] University of Connecticut.
[‡] Vanderbilt University.

10.1021/ma0706125 CCC: $37.00
Published on Web 06/12/2007

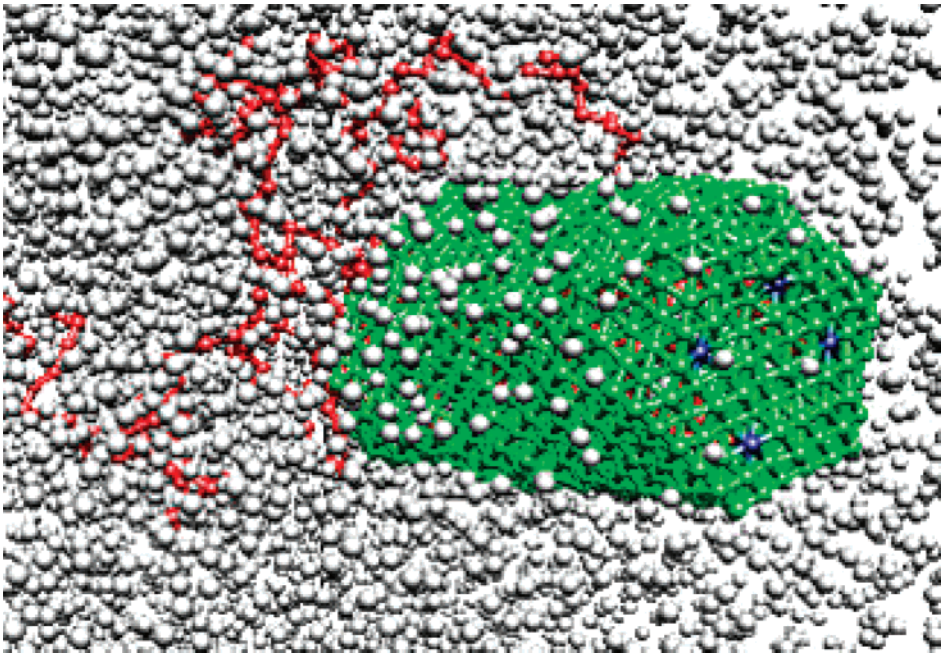

Figure 1. Snapshot of the nozzle in solution. Monomers forming nozzle surface are shown in green, polymerization centers are colored in blue, growing polymer chains are shown in red, and surrounding nozzle solvent molecules are shown in light gray. Note that the most of the solvent molecules located in front of the nozzle in the simulation box are removed to make a clear view of the nozzle.

shifted Lennard-Jones (LJ) potential with the cutoff distance, $r_{cut} = \sqrt[6]{2}\sigma$, and the interaction parameter $\epsilon_{LJ} = k_B T$.

$$U_{LJ}(r_{ij}) = \begin{cases} 4\epsilon_{LJ}\left[\left(\frac{\sigma}{r_{ij}}\right)^{12} - \left(\frac{\sigma}{r_{ij}}\right)^{6} - \left(\frac{\sigma}{r_{cut}}\right)^{12} + \left(\frac{\sigma}{r_{cut}}\right)^{6}\right], r \le r_{cut} \\ 0\ , r > r_{cut} \end{cases} \quad (2)$$

This choice of parameters corresponds to a purely repulsive LJ potential.

The simulations were performed with explicit solvent with concentration $c = 0.1\sigma^{-3}$ (see Figure 2). In our simulations we used periodic boundary conditions with simulation box size $L = 60\sigma$. Simulations were carried out in a constant temperature ensemble. Constant temperature was maintained by coupling the system to a Nose-Hoover thermostat, which preserves hydrodynamic modes.[27] In this case, the equation of motion for the ith bead is

$$m\frac{d\vec{v}_i}{dt}(t) = \vec{F}_i(t) + \vec{F}_i^{T}(t) \quad (3)$$

where $\vec{v}_i$ is the bead velocity, $\vec{F}_i$ is the net deterministic force acting on ith bead of mass m, and $\vec{F}_i^{T}(t)$ is a force coupling the system to a thermostat.[27] The velocity-Verlet algorithm[27] with a time step (MD time step) $\Delta t = 0.002\tau_{LJ}$ was used to integrate the equations of motion (3), where τ_{LJ} is the standard LJ time, $\tau_{LJ} = \sigma(m/k_B T)^{1/2}$. Each simulation run lasted 2.5×10^7 integration steps.

Growing polymer chains were permanently attached to catalytic sites that were uniformly distributed over the nozzle cap. We have performed simulations with 1, 2, 4, 6, and 8 polymerization centers. The chain polymerization was performed as follows: a reactive monomer located outside the nozzle within a capture radius from a polymerization site was selected and inserted as a pointlike monomer into polymer chain; a point bead was generated between the catalytic site and the first bead of the polymer chain with a velocity randomly picked from the Maxwell distribution. The size of a bead grows at a rate of $0.01/\Delta t$. After a polymer chain achieved a degree of polymerization $N_p = 100$, its length N_p was kept constant for the rest of the simulation run by removing a bond connecting a monomer at the terminal end as new monomer was added to the chain. This prevented depletion of the number of monomers during the simulation run. Note that the presence of the explicit monomers in a system at given concentration and the size of the capture radius determine the rate at which new monomers were added to growing polymer chains. In our simulations the capture radius was equal to 1.25σ, 1.5σ, and 1.75σ. Figure 2 shows the evolution of the chain growth during the simulation run.

It is important to point out that the simulations of the nanopropulsion engine presented in this paper correspond to the Zimm (nondraining) dynamics[23−25] of the moving nozzle and growing polymer chains. This is achieved by implementing the Nose-Hoover thermostat to maintain the system temperature. In this respect these simulations are different from the ones presented in our previous paper[28] in which we have studied the Rouse (free draining) dynamics[23−25] of the nozzle motion.

Figure 3 shows a linear relationship between the nozzle velocity and chain's polymerization rate R_p for nozzles of fixed geometries. The data points for this plot were obtained by fitting the mean-square displacement $\langle \Delta r(t)^2 \rangle$ of the center of mass of the nozzle to the following equation

$$\langle \Delta r(t)^2 \rangle = 2v_t^2\tau_p t - 2v_t^2\tau_p^2(1 - \exp(-t/\tau_p)) \quad (4)$$

describing the motion of an object with a constant average velocity v_t which orientational correlations decay exponentially, $\langle \vec{v}(t)\vec{v}(t + \Delta t) \rangle = v_t^2 \exp(-\Delta t/\tau_p)$, with characteristic time τ_p. The loss of the orientational correlations is due to fluctuations of the direction of the propulsive force caused by the nozzle shape fluctuations that are determined by the nozzle rigidity and compressibility of the polymeric solution inside the nozzle. Note that during the time intervals $t < \tau_p$ the motion of the nozzle is ballistic with $\langle \Delta r(t)^2 \rangle \approx v_t^2 t^2$ while at longer time intervals $t > \tau_p$ the motion is diffusion-like, $\langle \Delta r(t)^2 \rangle \approx 2v_t^2\tau_p t$, with the effective diffusion coefficient $D = v_t^2\tau_p/3$. The

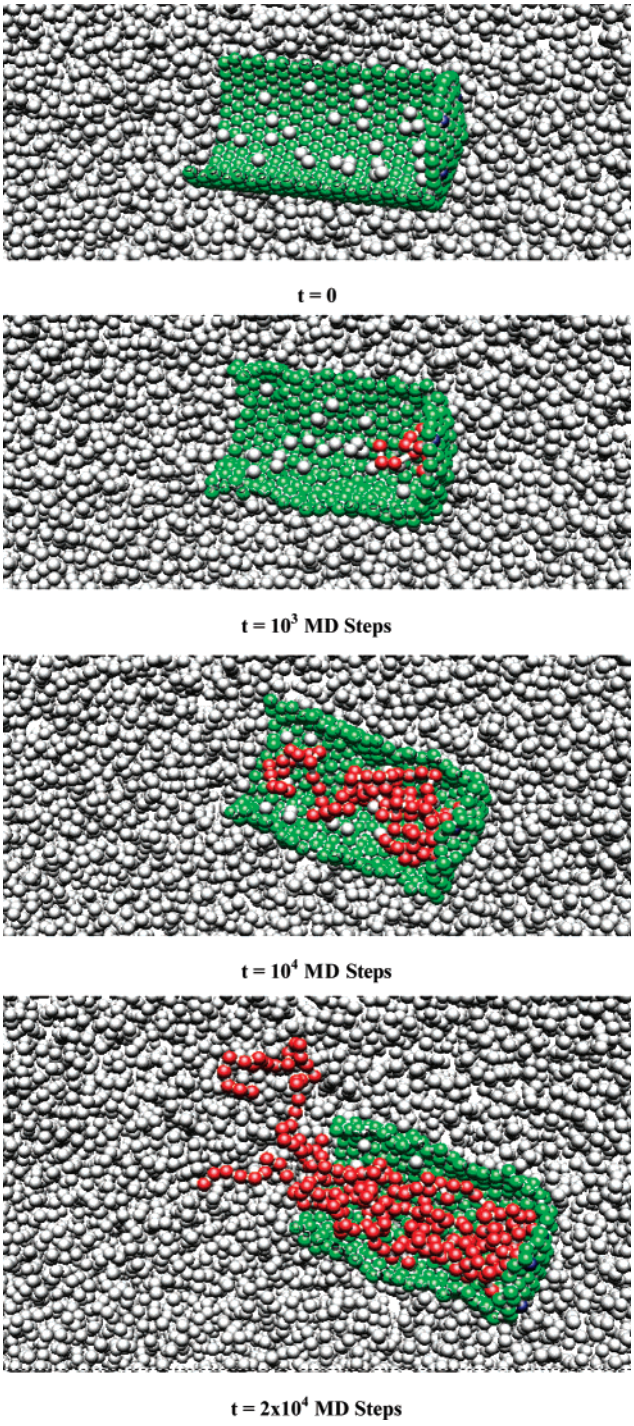

Figure 2. Evolution of the growing polymer chains inside a cylindrical nozzle (C30L20) during the simulation run. Monomers forming nozzle are shown in green, polymerization centers are shown in blue, growing polymer chains are shown in red, and the solvent molecules are shown in light gray.

existence of the constant average velocity v_t is an indication of the constant propulsive force acting on the nozzle. As one would expect, the magnitude of this force is larger for the faster polymerization rates R_p and is manifested by the faster motion of the nozzle. The nozzle velocity also depends on the geometric characteristics of a nozzle such as its length and size. The larger nozzle moves slower than the smaller ones at the same polymerization rate R_p.

To establish how this propulsion motion is related to the nozzle geometry, we modified a scaling model describing the

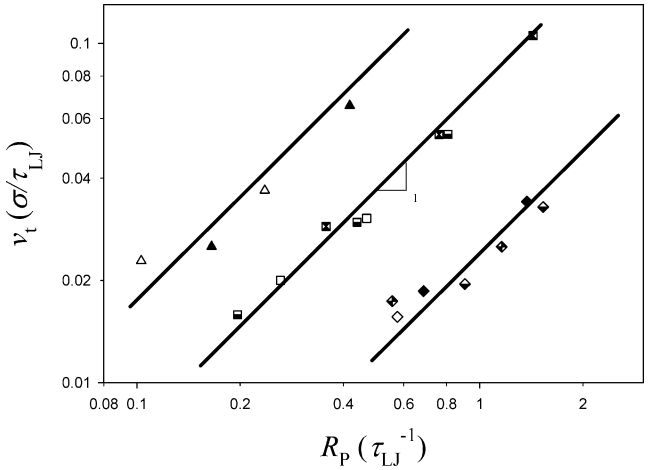

Figure 3. Dependence of the nozzle average velocity on the net polymerization rate for the nozzles of different geometries: C18L20P1, open triangles; C18L20P2, filled triangles; C30L20P1, open squares; C30L20P2, semifilled squares; C30L20P4, square with hourglass; C54L20P1, open diamonds; C54L20P4, semifilled diamonds; C54L20P6, diamonds with hourglass; C54L20P8, filled diamonds. *P* denotes the number of polymerization centers on the nozzle cap.

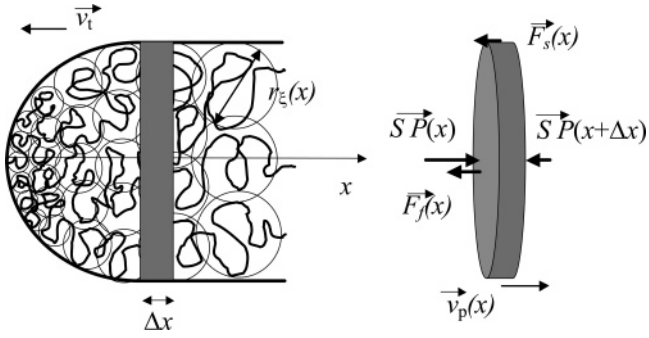

Figure 4. Schematic representation of blob structure of polymer chains inside a nozzle and of the forces acting on the slice of polymer solution.

nozzle motion to take into account the hydrodynamic interactions.[28] Consider a nozzle with radius R and length l moving with an average velocity v_t (see Figure 4). Let us choose a moving system of coordinates associated with a nozzle and select the direction of the x-axis along the cylindrical axis of the nozzle, pointing toward its open end. The monomers are constantly inserted into polymer chains at the closed end of the nozzle with the net polymerization rate R_p. In a steady-state regime, the distribution of polymers inside the nozzle is given by the density profile $\rho(x)$. This polymer density profile sets up the distribution of the polymeric osmotic pressure $P(x)$ along the x-axis. We will assume that polymer mass is pushed toward the open end of the nozzle as a plug and will neglect the radial variations in the polymer density distribution. Thus, all monomers which are located at the distance x from the origin of the moving frame have an average velocity $v_p(x)$ relative to the moving frame. In the steady-state regime the polymeric mass is moving through the nozzle without acceleration. Thus, the sum of all forces acting on the slice of polymer solution with thickness Δx and area $S = \pi R^2$ is equal to zero (see Figure 4). This slice is pushed toward the open end of the nozzle by the force generated by the polymeric pressure difference on both sides of the slice

$$F_{pol}(x) = S(P(x) - P(x + \Delta x)) \approx -S\Delta x \frac{\partial P(x)}{\partial x} \qquad (5)$$

This force is opposed by the friction of this slice against solvent $F_f(x)$ and by the sliding friction force $F_s(x)$ against the nozzle surface.

The analysis of the polymer density profile inside the nozzle shows that polymer chains inside a nozzle form semidilute or concentrated polymer solutions. In such solutions the hydrodynamic interactions are exponentially screened at length scales larger than the solution correlation length r_ξ (correlation blob size).[23−25] The hydrodynamic interactions between different parts of the chain subsections control its dynamics at the length scales shorter than the correlation length r_ξ. The motion of these subsections is described in the framework of the Zimm model.[23−26] Because of the exponential screening of the hydrodynamic interactions at length scales longer than the solution correlation length r_ξ, the polymer chain behaves as a Rouse chain of beads whose size is equal to the solution correlation length r_ξ. The friction coefficient of the blob against solvent is equal to

$$\xi_{blob} \approx 6\pi\eta r_\xi \approx \xi r_\xi/\sigma \tag{6}$$

where η is the solvent viscosity and $\xi = 6\pi\eta\sigma$ is the effective monomeric friction coefficient.

In the case of the nonuniform polymer density profile $\rho(x)$ the correlation blob size $r_\xi(x)$ and the number of monomers in correlation blob $g(x)$ are varying along the x-axis. For polymer chain in a good solvent for the polymer backbone, there is a following relation between the blob size $r_\xi(x)$ and the number of monomers in it $g(x)$

$$r_\xi(x) \propto \sigma g(x)^\nu \tag{7}$$

where $\nu = 0.588$ is the good solvent exponent.[23−25] In semidilute polymer solution the blobs are densely packed such that

$$\rho(x) \propto \frac{g(x)}{r_\xi(x)^3} \propto \sigma^{-3} g(x)^{1-3\nu} \tag{8}$$

Solving this equation for the number of monomers in a blob $g(x)$ as a function of the local polymer volume fraction $\varphi(x) = \rho(x)\sigma^3$, one has

$$g(x) \propto \varphi(x)^{1/(1-3\nu)} \tag{9}$$

In solution of blobs, the friction coefficient of the slice of a polymer chain with thickness Δx is proportional to the total number of blobs within volume $S\Delta x$, which is equal to $\rho(x)S\Delta x/g(x)$, times the blob friction coefficient $\xi r_\xi(x)/\sigma$. The projection on the x-axis of the friction force against solvent is equal to the slice friction coefficient times the velocity difference between the polymer and solvent $v_p(x) - v_t$

$$-F_f(x) \propto -(v_p(x) - v_t)\frac{\xi r_\xi(x)}{\sigma}\frac{\rho(x)S\Delta x}{g(x)} \propto -\left(\frac{R_p\xi}{S}\varphi(x)^{(1-\nu)/(3\nu-1)} - \frac{v_t\xi}{\sigma^3}\varphi(x)^{(2\nu)/(3\nu-1)}\right)S\Delta x \tag{10}$$

In derivation of the eq 10, we use a steady-state condition that the polymeric flux through each cross section area is equal to the chain polymerization rate, $v_p(x)\rho(x)S = R_p$.

The friction force between the surface of the nozzle and the polymer is proportional to the relative velocity $v_p(x)$ between the nozzle surface and the growing polymer. We will assume that the sliding friction coefficient is equal to $\xi_s r_\xi(x)/\sigma$ and that only those blobs that are within thickness δ from the surface of the nozzle experience this friction. The projection of the sliding friction force on the x-axis is equal to

$$-F_s(x) \propto -v_p(x)2\pi R\delta\frac{\xi_s r_\xi(x)\,\rho(x)}{\sigma g(x)}\Delta x \propto -R_p\xi_s\frac{2\delta}{R}\varphi(x)^{(1-\nu)/(3\nu-1)}\Delta x \tag{11}$$

Taking into account new expressions for the friction forces given by eqs 10 and 11, we can write the following differential equation describing distribution of the polymer density inside the nozzle as a function of the nozzle average velocity v_t and the chain polymerization rate R_p

$$-\frac{\partial P(x)}{\partial x} \propto -\frac{v_t\xi}{\sigma^3}\varphi(x)^{2\nu/(3\nu-1)} + \frac{R_p}{S}\left(\xi + \xi_s\frac{2\delta}{R}\right)\varphi(x)^{(1-\nu)/(3\nu-1)} \tag{12}$$

This equation describes the distribution of the polymeric osmotic pressure and the polymer density inside nozzle. In polymer solution the polymeric osmotic pressure depends on the local polymer density as $P(x) \approx k_B T\varphi(x)^{3\nu/(3\nu-1)}/\sigma^3$.[23−25]

To obtain the expression for the nozzle velocity, we have to write the equation describing the motion of the nozzle itself. In the steady state the sum of all forces acting on the nozzle also should be equal to zero. These forces include the net force exerted by the confined polymer solution on the surface of the nozzle cap $SP(0)$, pointing toward the direction of the nozzle motion, the friction force between nozzle and solvent $-v_t\xi_t$, and the net sliding friction force F_s^n between the nozzle surface and the growing polymers which direction coincide with the nozzle velocity. For a cylindrical nozzle of radius R and length l moving along its long axis, the friction coefficient is equal to[26]

$$\xi_t = \frac{2\pi\eta l}{\ln(l/2R)} \tag{13}$$

The magnitude of the net sliding friction force F_s^n between the nozzle surface and polymer chain is obtained by summing contributions from all sliding friction forces acting along the whole length l of the nozzle

$$F_s^n(x) \propto \int_0^l v_p(x)2\pi R\delta\frac{\xi_s r_\xi(x)\,\rho(x)}{\sigma g(x)}\,dx \propto R_p\xi_s\frac{2\delta}{R}\int_0^l\varphi(x)^{(1-\nu)/(3\nu-1)}\,dx \tag{14}$$

Combining all contributions together, we can write the following equation describing nozzle motion

$$P(0)S \propto \xi_t v_t + R_p\xi_s\frac{2\delta}{R}\int_0^l\varphi(x)^{(1-\nu)/(3\nu-1)}\,dx \tag{15}$$

In the general case, in order to obtain the relation between the nozzle velocity and chain polymerization rate, we have to solve eqs 12 and 15. However, in the limit when the polymeric pressure at the open end of the nozzle $P(l)$ is small such that $P(0)/P(l) \gg 1$, we can integrate eq 12 between 0 and l and obtain another equation relating the polymeric pressure $P(0)$, nozzle velocity v_t, and chain polymerization rate R_p. Eliminating $P(0)$

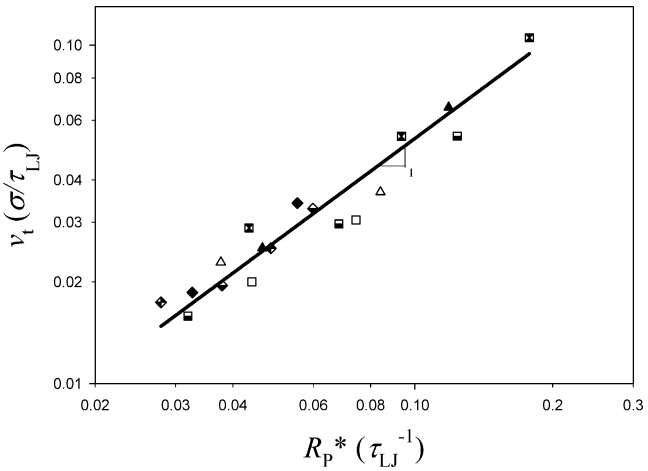

Figure 5. Dependence of the average nozzle velocity on the reduced polymerization rate R_p*. The symbol notations are the same as in Figure 2.

from these equations, we can write the expression relating the nozzle velocity with the polymerization rate

$$v_t \propto R_p^* \approx R_p \frac{\xi \int_0^l \varphi(x)^{(1-\nu)/(3\nu-1)}\,dx}{\xi_t + \frac{S\xi}{\sigma^3}\int_0^l \varphi(x)^{(2\nu)/(3\nu-1)}\,dx} \qquad (16)$$

Thus, the velocity of the nozzle is proportional to the polymerization rate with the proportionality coefficient being dependent on the nozzle friction coefficient, nozzle length, and the polymer density profile inside the nozzle.

Figure 5 confirms the linear relation between the nozzle velocity v_t and the reduced polymerization rate R_p*. This choice of the reduced variables allows collapse of all simulation data shown in Figure 3 into one universal plot. To obtain this plot, we have performed numerical integration of the average polymer density profile inside a nozzle and set $\nu = 0.6$.[23,24] This universal plot validates the proposed mechanism for the nozzle propulsion motion. Note that the relation eq 16 describing the Zimm dynamics of the moving nozzle is qualitatively different from the one obtained for the nozzle obeying the Rouse dynamics.[28] In the case of the Rouse dynamics the nozzle velocity is inversely proportional to the sum of the total number of monomers inside the nozzle and the number of monomer forming a nozzle. This is due to the absence of the hydrodynamic interactions between monomers in the Rouse model, which results in independent contribution of each monomer to the net nozzle friction coefficient. Thus, in the case of the Rouse dynamics the effective friction coefficient of the nozzle is proportional to the net nozzle mass while in the case of the Zimm dynamics the effective friction coefficient depends on the nozzle geometric characteristics such as its length and width and distribution of the monomer density inside the nozzle.

To the end let us comment on the finite chain length used in simulations. The presented above analysis shows that the nozzle velocity only depends on the distribution of the monomer density inside the nozzle. Thus, as long as the number of monomers in the polymer chain is larger than the number of monomers confined inside the nozzle, we do not expect any significant effect of the finite chain length on the nozzle motion. Note that the increase of the number of monomers in a polymer chain beyond $N_p = 100$ can only slightly influence the nozzle motion due to renormalization of the local solution viscosity outside the nozzle by the sections of the growing polymer chains.

In conclusion, we have proposed a model of the polymeric nanopropulsion engine, which can generate a directional motion in a solution by polymerizing macromolecules inside nozzlelike pores. The engine can be thought of as an analogue of the jet propulsion engine, which secretes polymers in a solution and takes advantage of the polymer viscoelasticity to propel itself forward. The proposed design of the nanopropulsion engine is simple enough that its construction should be feasible using modern chemical techniques.

Acknowledgment. The authors are grateful to Profs. M. Rubinstein, R. Colby, E. Samulski, and J.-F. Joanny for useful discussions. This research was supported by the National Science Foundation under Grant DMR-0305203 and by the University of Connecticut Research Foundation.

Supporting Information Available: Movie of the nozzle motion during the simulation run. This material is available free of charge via the Internet at http://pubs.acs.org.

References and Notes

(1) Amos, L. A. *Nat. Chem. Biol.* **2005**, *1*, 319.
(2) Fletcher, D. A.; Theriot, J. A. *Phys. Biol.* **2004**, *1*, T1.
(3) Gehrig, E.; Hess, O. *Phys. Rev. E* **2006**, *73*, 051916.
(4) Mallik, R.; Carter, B. C.; Lex, S. A.; King, S. J.; Gross, S. P. *Nature (London)* **2004**, *427*, 649.
(5) Mogilner, A.; Oster, G. *Curr. Biol.* **2003**, *13*, R721.
(6) Spudich, J. A. *Cell* **2006**, *126*, 242.
(7) Wolgemuth, C. W.; Oster, G. *J. Mol. Microbiol. Biotechnol.* **2004**, *7*, 72.
(8) Schliwa, M.; Woehlke, G. *Nature (London)* **2003**, *422*, 759.
(9) Chiu, W.; Baker, M. L.; Almo, S. C. *Trends Cell Biol.* **2006**, *16*, 144.
(10) Xing, J. H.; Bai, F.; Berry, R.; Oster, G. *Proc. Natl. Acad. Sci. U.S.A.* **2006**, *103*, 1260.
(11) Kinbara, K.; Aida, T. *Chem. Rev.* **2005**, *105*, 1377.
(12) Gerbal, F.; Chaikin, P.; Rabin, Y.; Prost, J. *Biophys. J.* **2000**, *79*, 2259.
(13) Marcy, Y.; Prost, J.; Carlier, M.-F.; Sykes, C. *Proc. Natl. Acad. Sci. U.S.A.* **2004**, *101*, 5992.
(14) McBride, M. J. *Annu. Rev. Microbiol.* **2001**, *55*, 49.
(15) Berna, J.; et al. *Nat. Mater.* **2004**, *4*, 704.
(16) Hess, H.; et al. *Nano Lett.* **2003**, *3*, 1651.
(17) Reuther, C.; Hajdo, L.; Tucker, R.; Kasprzak, A. A.; Diez, S. *Nano Lett.* **2006**, *6*, 2177.
(18) Shirai, Y.; Morin, J.-F.; Sasaki, T.; Guerrero, J. M.; Tour, J. M. *Chem. Soc. Rev.* **2006**, *35*, 1043.
(19) Badjic, J. D.; et al. *J. Am. Chem. Soc.* **2006**, *128*, 1489.
(20) Badjic, J. D.; Balzani, V.; Credi, A.; Silvi, S.; Stoddart, J. F. *Science* **2004**, *303*, 1845.
(21) Dreyfus, R.; et al. *Nature (London)* **2005**, *437*, 862.
(22) Kumara, M. T.; Srividya, N.; Muralidharan, S.; Tripp, B. C. *Nano Lett.* **2006**, *6*, 2121.
(23) Grosberg, A. Y.; Khokhlov, A. R. *Statistical Physics of Macromolecules*; AIP Press: New York, 1994.
(24) Rubinstein, M.; Colby, R. H. *Polymer Physics*; Oxford University Press: New York, 2003.
(25) de Gennes, P.-G. *Scaling Concepts in Polymer Physics*; Cornell University Press: Ithaca, NY, 1985.
(26) Doi, M.; Edwards, S. F. *The Theory of Polymer Dynamics*; Clarendon Press: New York, 1986.
(27) Frenkel, D.; Smit, B. *Understanding Molecular Simulations*; Academic Press: San Diego, CA, 2001.
(28) Jeon, J.; Dobrynin, A. V. *Eur. Phys. J. E* **2005**, *17*, 361.

MA0706125